

Improved Thermoelectric Performance in n-type $\text{Bi}_2(\text{Te},\text{Se})_3$ Alloys through the Incorporation of Fe Nanoparticles

Kyungmi Lee, Gwansik Kim, Sung Wook Ye, Jeongmin Kim, Jong Wook Roh,* and Wooyoung Lee*

Cite This: *ACS Appl. Energy Mater.* 2024, 7, 9300–9306

Read Online

ACCESS |



Metrics & More



Article Recommendations

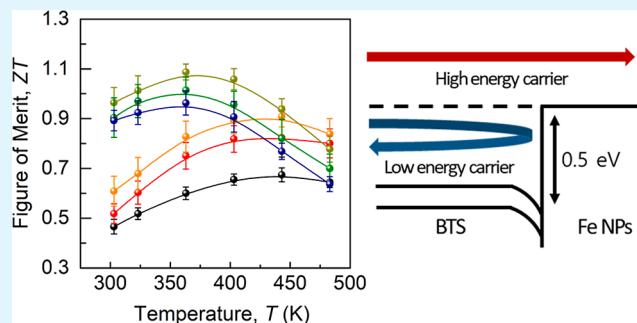


Supporting Information

ABSTRACT: Herein, we investigated the thermoelectric properties of Fe-BTS (Bi_2Te_3 -based compound) samples fabricated through nanometal decoration and spark plasma sintering. We examined the effects of Fe nanoparticle (NP) addition on the power factor (PF), thermal conductivity (κ), and figure of merit (ZT) of the samples. The incorporation of Fe NPs led to a significant increase in the PF of the Fe-BTS samples, surpassing the performance of the pristine sample by over 34%. This improvement is attributed to the combined effects of carrier concentration tuning and low-energy carrier filtering. Additionally, the thermal conductivity of the Fe-BTS samples was significantly reduced due to enhanced phonon scattering at the increased interfaces. Consequently, a maximum ZT value of 1.09 was achieved at 363 K for the Fe-BTS sample with an Fe content of 0.3 vol %.

These findings highlight the crucial role of interface engineering in enhancing the thermoelectric properties of materials.

KEYWORDS: thermoelectric materials, thermoelectric, sintering, nanostructured materials, electrical properties, $\text{Bi}_2(\text{Te},\text{Se})_3$



1. INTRODUCTION

The Seebeck effect, discovered in 1821, has sparked significant interest in the exploration of thermoelectric (TE) materials due to their ability to convert heat into electrical energy and vice versa. Over the years, the integration of nanotechnology and nanomaterials into the field of thermoelectrics has led to the development of more efficient and cost-effective thermoelectric materials and devices.^{1–5} As the demand for sustainable energy sources rises and the call for more efficient and environmentally friendly technologies grows, there has been a renewed interest in nanomaterial-based thermoelectrics. Among these materials, $\text{Bi}_2(\text{Te},\text{Se})_3$ (BTS) alloys have been extensively studied as well-known n-type thermoelectric materials with a high performance near room temperature.^{6–14} The thermoelectric properties of BTS can be finetuned by varying their composition and microstructure.^{15–17} Recently, the thermoelectric performance of BTS was enhanced by incorporating magnetic nanoparticles (NPs) into the matrix.^{18–24} Despite the introduction of such complex processes for enhancing the thermoelectric performance, dramatic improvements have been limited in n-type BTS thermoelectric materials due to the difficulty in optimization of power factor (PF).

The introduction of NPs to bulk BTS is an effective way to reduce the total thermal conductivity (κ_{total}) by acting as a phonon scattering source.^{25–27} Moreover, the incorporation of magnetic NPs have been one of methods to increase the Seebeck coefficient (S) of thermoelectric materials through the

interaction between the spin of the electric carriers and magnetic field of the nanoparticles.^{18,28,29} As a result of synergetic effect that caused by the reduced thermal conductivities and enhanced Seebeck coefficient, the thermoelectric figure of merit ($ZT = \sigma S^2 T / \kappa_{\text{total}}$, where T is temperature) can be strengthened by the introduction of magnetic NPs. Herein, the TE properties of Fe-BTSs fabricated by simple methods of Fe NPs introduction and spark plasma sintering (SPS) were investigated. The PF of the Fe-BTS samples increased by >34% compared with that of the pristine sample. Moreover, the κ of these samples decreased owing to the intensified phonon scattering caused by the increased interface density and multiple phonon scattering.

2. EXPERIMENTAL SECTION

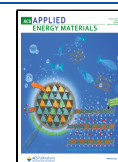
The Fe-BTS samples (Fe 0.1–0.5 vol %) were synthesized by the nanometal decoration technique^{30–33} and SPS method. Zone-melted commercial BTS ingots were utilized to synthesize the BTS matrix materials (LIVINGCARE Co., Ltd.). The BTS ingots were pulverized into powders using a ball mill (Pulverisette 7) for 10 min under an Ar atmosphere to prevent oxidation of the pristine powder. To decorate

Received: July 9, 2024

Revised: October 9, 2024

Accepted: October 10, 2024

Published: October 15, 2024



Fe NPs on the surface of BTS powders, iron (II) acetate $[(\text{CH}_3\text{COO})_2\text{Fe}]$, Alfa Aesar] and sieved BTS powder were mixed using a high energy ball milling process for 5 min under Ar atmosphere. Mixed powders of iron(II) acetate and BTS-based powders were annealed at 473 K for 3 h under a mixed gas atmosphere (95% N_2 and 5% H_2) to remove the acetate ($-\text{CH}_3\text{COO}^-$). The annealed powder was sintered via SPS at 773 K for 2 min under 30 MPa in a vacuum using a graphite die with a diameter of 10 mm.

X-ray diffraction (XRD, Ultima IV/ME 200DX) with $\text{CuK}\alpha$ radiation was used to characterize the phase formation of the samples. The lattice parameters were calculated using Rietveld refinement. High resolution transmission electron microscopy (HRTEM) and energy dispersive spectrometry (EDS) were performed using an instrument for field emission transmission electron microscopy (FE-TEM, Titan G2 ChemiSTEM Cs Probe) to determine the size and position of the Fe NPs in the Fe-BTS samples.

The thermoelectric properties were measured on the plane perpendicular to the pressing direction. The temperature dependence of σ and S of the Fe-BTS samples was measured using a commercial TE measurement instrument (ZEM-3) within the range of 303–483 K under low pressure He gas. The κ_{tot} values were calculated using the equation $\kappa_{\text{tot}} = \rho_s C_p \lambda$, where ρ_s is the density, C_p is the specific heat capacity, and λ is the thermal diffusivity. λ was determined using the laser flash method (LFA-457) under vacuum from 303–483 K, and the C_p value was constant at $0.157 \text{ J g}^{-1} \text{ K}^{-1}$. Hall effect measurements were performed in a van der Pauw configuration under a constant magnetic field (1 T) at 303 K. The carrier concentration (n_c) and carrier mobility (μ_{Hall}) were estimated using a one-band model, disregarding the minority carriers. The work function of the BTS sample was estimated using ultraviolet photoemission spectroscopy (UPS, ESCALAB 250Xi) with a He(I) radiation source ($h\nu = 21.2 \text{ eV}$). The magnetic properties of the Fe-BTS samples were measured using a vibrating sample magnetometer (VSM, 8600 Series VSM) at room temperature.

3. RESULTS AND DISCUSSION

The microstructures under several Fe-BTS conditions were investigated to reveal the relationship between the microstructure and thermoelectric properties. Figure 1a presents the XRD patterns of the Fe-BTS samples (Fe 0–0.5 vol %). All the patterns coincided with the rhombohedral $R\bar{3}m$ space group as the major phase, and the lattice parameters for all the samples were similar. The diffraction peaks from Fe NPs are not detected in the Fe-BTS samples due to their low concentration.

Figure S1 shows the SEM and EDS images of the fractured surfaces of the Fe-BTS samples. The compacted polycrystalline bulks, exhibiting fine-layered and clean microstructures, are shown in Figure S1. The grain size of the nanocomposites gradually decreased from $>10 \mu\text{m}$ (pristine) to $3 \mu\text{m}$ (0.5 vol % Fe-BTS sample), suggesting that the Fe NPs act as the grain growth inhibitor in grain boundaries.^{34,35} However, the grain growth inhibition by Fe NPs exerted no effect on the TE properties because the microsized grains did not significantly affect phonon and electron transport. In addition, we observed that the Fe content became more evenly distributed as the amount of Fe NPs increased, whereas the atomic contents of Bi, Te, and Se remained constant. To investigate the size and location of Fe NPs in the 0.5 vol % Fe-BTS sample after the SPS process, TEM was performed. As shown in Figure 2a, Fe NPs were observed at the grain boundaries in the scanning transmission electron microscopy-high-angle annular darkfield (STEM-HAADF) image. Notably, the TEM-EDS images in Figure 2b show Fe NPs with diameters $>100 \text{ nm}$ at the grain boundaries as well as well-dispersed Fe atoms within the BTS

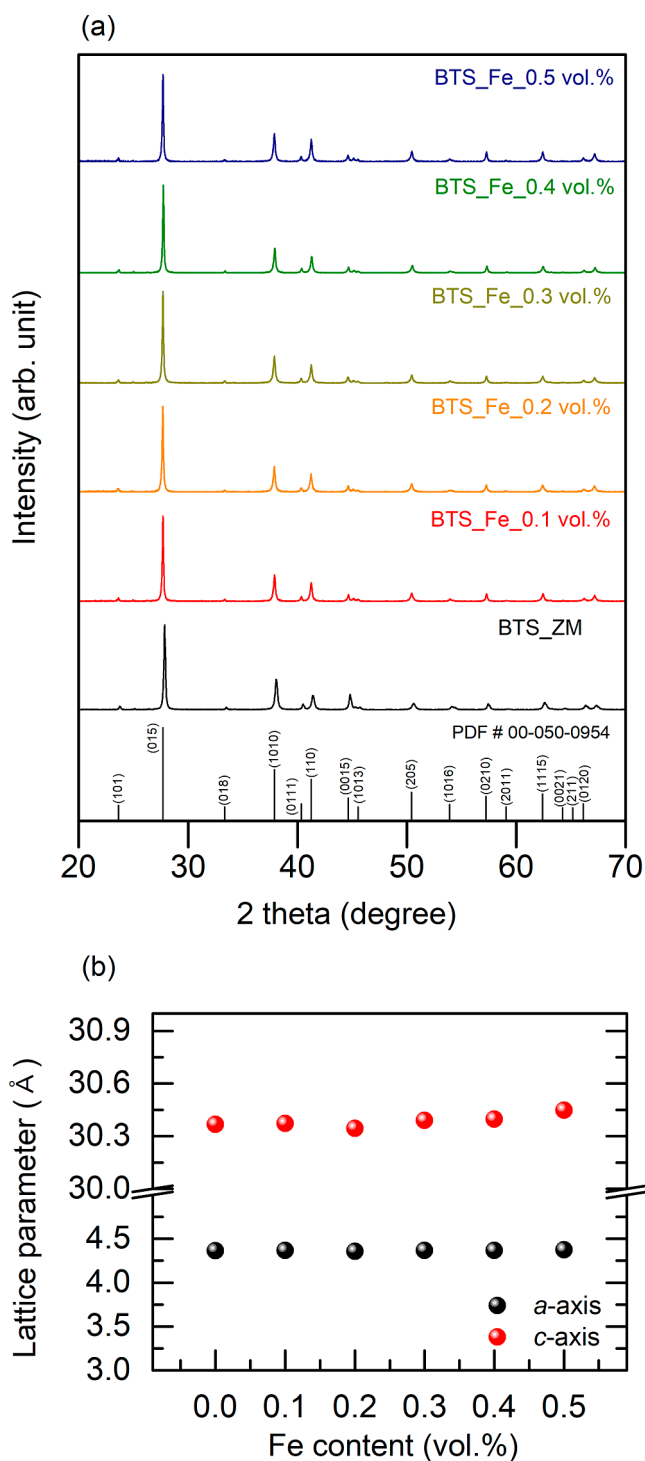


Figure 1. (a) XRD patterns and (b) lattice parameters a and c of Fe-BTS samples (Fe 0.1–0.5 vol %).

matrix. At lower Fe content ($\leq 0.2 \text{ vol } \%$), the SPS process facilitated the diffusion of Fe atoms into the BTS matrix (Figure S2). However, at higher Fe content ($\geq 0.3 \text{ vol } \%$), the presence of Fe NPs at the grain boundaries could be attributed to diffusion suppression or precipitation, depending on the solubility limit.

In this study, the mechanisms of Fe diffusion were elucidated by investigating the electron and thermal transport properties. The temperature dependences of σ , S , PF, κ , and ZT of the Fe-BTS samples were assessed to examine the

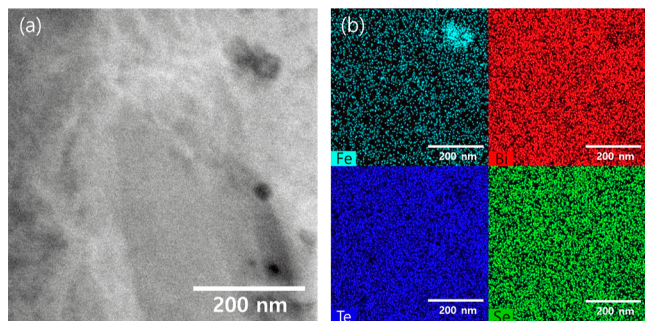


Figure 2. (a) STEM-HAADF image and (b) STEM-EDS image of the 0.5 vol % Fe-BTS sample.

influence of Fe addition on their thermoelectric properties (Figure 3).

The σ of the Fe-BTS samples initially increased with increasing Fe content up to 0.2 vol %, but started to decrease for higher Fe content (≥ 0.3 vol %) indicating the optimum point. The increase in σ at lower Fe content (≤ 0.2 vol %) is due to Fe atoms diffusing into the BTS matrix, where they act as n-type dopants, resulting in an increase in n_c (Table 1). However, as the Fe content increases, the Fe NPs begin to inhibit diffusion or precipitate, leading to a decrease in σ . All the BTS samples showed negative S throughout the measured temperature range, which is characteristic of n-type semiconductor behavior. Notably, the S values of the Fe-BTS samples increased with higher Fe content (≥ 0.3 vol %), while the samples with lower Fe content (≤ 0.2 vol %) exhibited similar S values to the pristine sample. The S values of Fe-BTS samples reached the maximum point of $210.9 \mu\text{V K}^{-1}$ at $T = 363$ K for 0.5 vol %. This increase is due to scattering of the low energy carriers at the interface between the BTS matrix

and Fe NPs with band bending. In addition, the electronics transport properties, particularly the S , are affected by multiple scattering caused by the randomly turned magnetic moment due to the superparamagnetism of the Fe NPs.^{28,36} The magnetic properties of Fe-BTS samples are shown in Figure S3. To further clarify this observation, we calculated the n_c and μ_{Hall} at room temperature from the Hall-effect measurements by applying the one-band model, disregarding the minor carriers, as shown in Table 1.

The n_c values of the low-Fe-content BTS samples (8.0×10^{19} and $7.3 \times 10^{19} \text{ cm}^{-3}$ for 0.1 and 0.2 vol % Fe-BTS samples, respectively) were higher than that of the pristine samples. Conversely, the high Fe content samples had lower carrier concentrations (ranging from 2.5×10^{19} to $4.1 \times 10^{19} \text{ cm}^{-3}$) compared to the pristine sample. In addition, an inverse relationship between n_c and μ_{Hall} was observed, indicating that electron-electron scattering dominates the carrier transport.³⁷ The DOS (density of state) effective mass value (m_d^*) was calculated based on the electronic transport properties. The m_d^* was obtained from the measured S and n_c values using eq 1.

$$S = \frac{8\pi^2 k_B^2}{3eh^2} \left(\frac{\pi}{3n} \right)^{2/3} m_d^* T \quad (1)$$

where k_B , h , and e are the Boltzmann constant, Planck's constant, and elementary charge, respectively.^{38–40} Figure 4a shows S as a function of n_c for all the samples at 303 K. The solid lines were calculated for $m_d^* = 0.9, 1.2, 1.3,$ and $1.5 m_0$. As shown in the Pisarenko plot (Figure 4a), the m_d^* changed significantly with the amount of Fe added. Notably, the m_d^* slightly increased from $0.98 m_0$ (pristine sample) to 1.08 – $1.11 m_0$ (0.1 and 0.2 vol % Fe-BTS samples) by a small amount (≤ 0.2 vol %) of Fe doping. Thus, the PF in the inset of Figure 3b could be slightly enhanced owing to the synergetic effects of

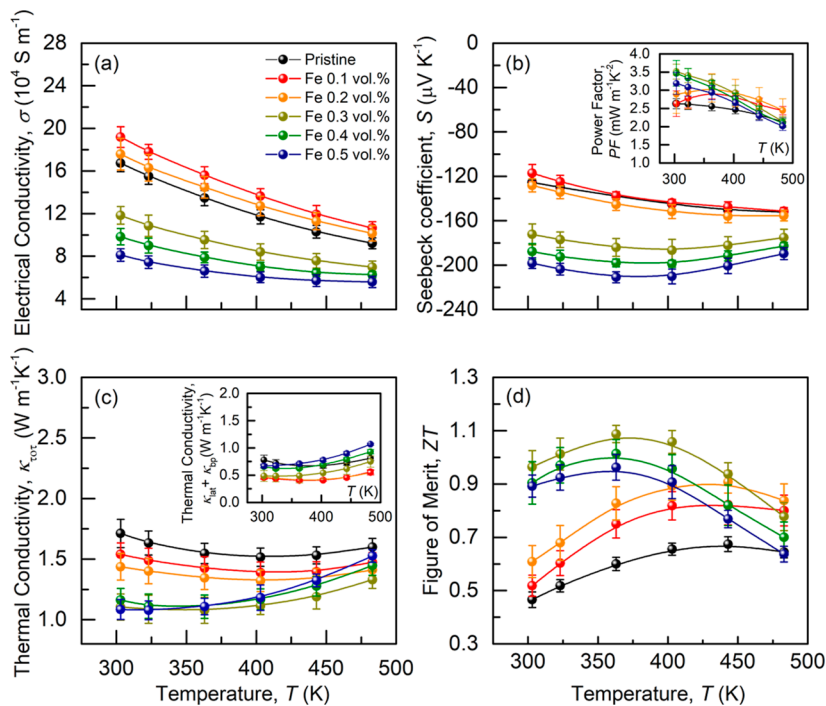
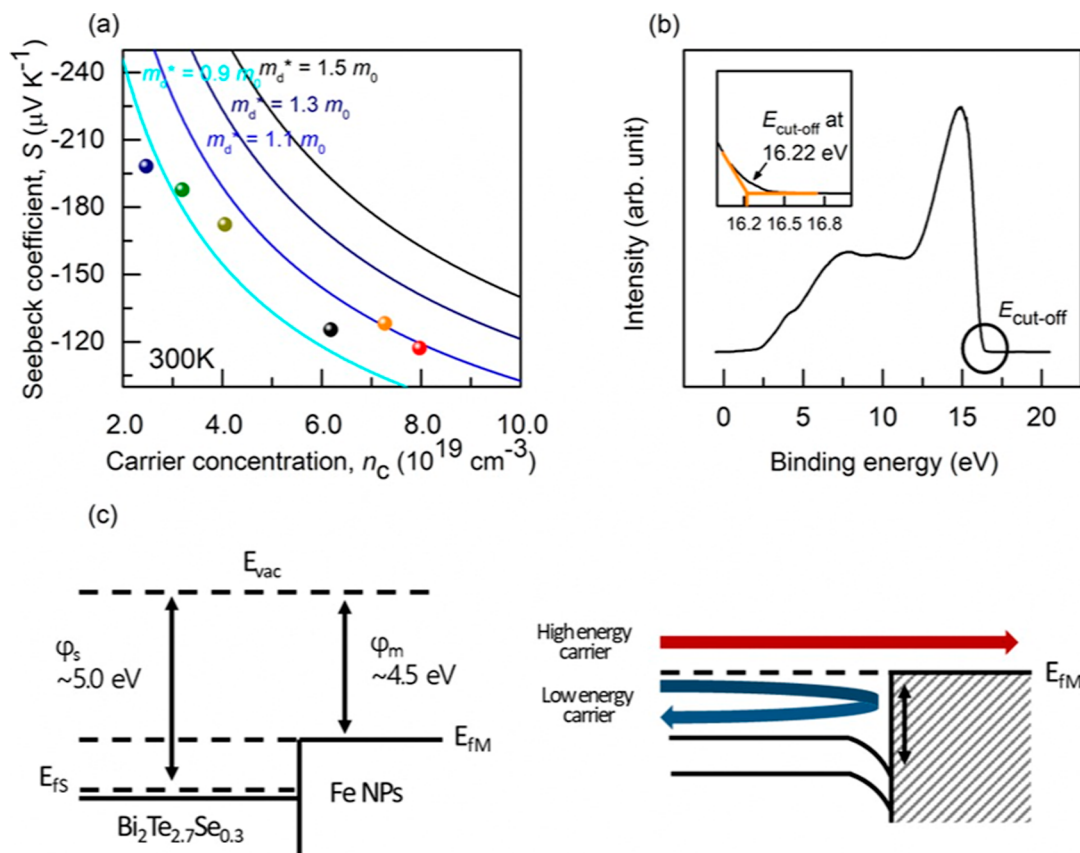


Figure 3. Temperature dependence (a) electrical conductivity (σ), (b) Seebeck coefficient (S), (c) thermal conductivity (κ), and (d) figure-of-merit (ZT) values of Fe-BTS samples (Fe 0–0.5 vol %). (Inset of (b): The calculated PF, inset of (c): the sum of the lattice and bipolar thermal conductivity ($\kappa_{\text{lat}} + \kappa_{\text{bp}}$)).

Table 1. Electric Conductivity (σ), Seebeck Coefficient (S), Carrier Concentration (n_c) and Mobility (μ_{Hall}) at 303 K of Fe-BTS Samples (Fe 0–0.5 vol %)

	Σ (10^4 S m^{-1})	S ($\mu\text{V K}^{-1}$)	n_c (10^{19} cm^{-3})	μ_{Hall} ($\text{cm}^2 \text{ V}^{-1} \text{ s}^{-1}$)
BTS	16.7 (± 0.8)	−125.4 (± 2.2)	6.2 (± 0.2)	166.5 (± 3.1)
BTS + 0.1 vol % Fe	19.2 (± 0.9)	−117.1 (± 7.8)	8.0 (± 0.3)	148.1 (± 2.5)
BTS + 0.2 vol % Fe	17.6 (± 1.4)	−128.1 (± 6.0)	7.3 (± 0.5)	148.6 (± 4.8)
BTS + 0.3 vol % Fe	11.8 (± 0.8)	−172.3 (± 9.4)	4.1 (± 0.4)	179.5 (± 3.2)
BTS + 0.4 vol % Fe	9.8 (± 0.7)	−187.8 (± 7.1)	3.2 (± 0.3)	189.7 (± 2.7)
BTS + 0.5 vol % Fe	8.1 (± 0.5)	−199.2 (± 4.8)	2.5 (± 0.2)	202.0 (± 4.2)

**Figure 4.** (a) Pisarenko plot of Fe-BTS samples (Fe 0–0.5 vol %), (b) UPS spectrum of the pristine BTS matrix, and (c) schematic of band structure and interface potential difference owing to low energy carrier filtering effect between the BTS matrix and Fe NPs.

the carrier concentration tuning and enhanced m_d^* because of the Fe doping.

Conversely, the m_d^* of the BTS sample with high Fe content (≥ 0.3 vol %) decreased from $1.01 m_0$ (0.3 vol % Fe-BTS sample) to $0.84 m_0$ (0.5 vol % Fe-BTS samples) depending on the Fe content. Based on XRD analysis, we observed that the crystal structures of all samples remained unchanged. Consequently, we assume that the observed reduction in m_d^* in the high-Fe-content BTS samples is primarily due to the pronounced interface effect between the BTS matrix and the Fe NPs precipitated at the grain boundaries.³⁷ To investigate this further, the interface potential difference was studied by comparing the work functions of the BTS matrix and the Fe NPs. The work function of the pristine BTS matrix was obtained from the following eq 2.

$$\phi = h\nu - E_{\text{cut-off}} \quad (2)$$

where $h\nu$ is the phonon energy and $E_{\text{cut-off}}$ is the binding energy of the cutoff (Figure 4b). When comparing the work functions of Fe (4.5 eV)⁴¹ and the BTS matrix (5.0 eV), a

difference was observed at the interface potential barrier.⁴² Figure 4c shows a schematic of the potential barrier formed at the interface between the BTS matrix and Fe NPs. This potential barrier causes a band-bending effect, leading to low-energy carrier filtering.^{30,35,37,43–46} The reduction in n_c in the high-Fe-content BTS samples can be ascribed to this low-energy carrier-filtering effect, wherein the low-energy carriers are filtered and trapped by the interfacial potential difference. Moreover, the significant increase in the μ_{Hall} and small m_d^* values, as shown in Table 1 and Figure 4a, provide clear evidence of the low-energy carrier filtering effect. Consequently, we achieved the enhanced PF values of $3.51 \text{ mW m}^{-1} \text{ K}^{-2}$ at 303 K and $3.23 \text{ mW m}^{-1} \text{ K}^{-2}$ at 363 K in the 0.3 vol % Fe-BTS samples. This improvement in the PF was ascribed to a significant increase in the S resulting from the low-energy filtering effect. When Fe NPs are dispersed in BTS, the low-energy filtering effect causes low-energy carriers to be filtered or scattered, resulting in high-energy carriers primarily contributing to conduction and thereby enhancing the S .³⁷ Low-energy carrier filtering allows for the selective trapping of

low-energy carriers, leading to an increase in thermopower and consequently enhancing the PF.

We measured the thermal transport properties of the Fe-BTS samples in the same direction as the electronic transport properties. Figure 3c shows κ_{tot} as a function of the temperature for the Fe-BTS samples. Across the entire measured temperature range, the κ_{tot} values of all the Fe-BTS samples were lower than those of the pristine sample. In addition, the reduction in the majority of carriers (electrons) caused the minimum peak of κ_{tot} to shift from higher temperatures to room temperature owing to the enhanced contribution of bipolar thermal conduction. The $\kappa_{\text{lat}} + \kappa_{\text{bp}}$ value was calculated to confirm the phonon scattering effect. We estimated the κ_{ele} value using the Wiedemann–Franz law ($\kappa_{\text{ele}} = L\sigma T$), where L represents the Lorenz number, calculated using eq 3

$$L = 1.5 + \exp\left[-\frac{|S|}{116}\right] \quad (3)$$

where L and S are $10^{-8} \text{ W } \Omega \text{ K}^{-2}$ and $\mu\text{V K}^{-1}$, respectively.⁴⁷ The inset of Figure 3c shows the temperature dependence of $\kappa_{\text{lat}} + \kappa_{\text{bp}}$ for the Fe-BTS samples. Most $\kappa_{\text{lat}} + \kappa_{\text{bp}}$ values for the Fe-BTS samples were lower than those of the pristine sample owing to intensified phonon scattering (point defects, nanoprecipitation, and grain boundaries), particularly at 303 K. The introduction of Fe NPs could cause intensified multiscale phonon scattering from the atomic-scale (point defects) to the microscale (nanoprecipitation and grain boundaries).⁴⁸ In addition, the magnetic properties of Fe NPs could affect their thermal transport properties. The magnetic properties of the Fe-BTS samples are shown in Figure S3. The Fe-BTS samples exhibited superparamagnetic behavior owing to magnetic impurity doping or Fe NPs precipitation. The presence of superparamagnetic Fe NPs poses a challenge to their integration into BTS lattice due to fight against the spin splitting. Consequently, the reduction of lattice defects with the addition of Fe NPs leads to a decrease in the $\kappa_{\text{lat}} + \kappa_{\text{bp}}$ values at low temperatures.

Although the κ_{lat} values of these samples were reduced by integrated scattering, some Fe-BTS samples exhibited high $\kappa_{\text{lat}} + \kappa_{\text{bp}}$ values due to the cancellation of bipolar thermal conduction resulting from the low n_c values. Additionally, the increase in $\kappa_{\text{lat}} + \kappa_{\text{bp}}$ values at higher temperatures is due to the bipolar diffusion effect, resulting from the thermal activation of charge carriers trapped by the interfacial potential.³⁷ Therefore, higher ZT values were obtained for all Fe-BTS samples over a wide temperature range. The 0.3 vol % Fe-BTS sample achieved a maximum ZT value of 1.09 at 363 K. Considering the ZT values of the pristine sample, 0.3 vol % Fe-BTS sample exhibits increased values by >93% and >75% at 303 and 363 K, respectively. This enhancement in ZT for the Fe-BTS samples was realized by simultaneously controlling the electronic and thermal transport properties. This suggests that enhancing the TE properties through the introduction of magnetic metal NPs can be effectively achieved by precisely controlling the interface potential barrier.

4. CONCLUSION

In our comprehensive exploration of the TE properties, we researched into the unique characteristics exhibited by the Fe-BTS samples, precisely fabricated through the integration of Fe nanometal decoration and SPS processes. Notably, the PF of

these Fe-BTS samples exhibited a remarkable increase of more than 34% when compared to the pristine sample. This enhancement could be ascribed to the synergistic effects stemming from both of n_c tuning and low-energy filtering. The interesting aspect of this improvement lies in the involved interplay of factors. The n_c tuning synergized with the low-energy filtering, resulting in a collective boost to the PF. Furthermore, our investigation revealed a concurrent reduction in thermal conductivity (κ) for the Fe-BTS samples. This reduction in thermal conductivity is ascribed to the intensified scattering of phonons induced by two primary factors: the increased interface density within the material and the occurrence of multiple scattering events. The intricate interplay of these factors, intricately manipulated through the fabrication processes, leads to a notable decrease in thermal conductivity. As a cumulative effect of the increased PF and reduced thermal conductivity, the Fe-BTS samples achieved an impressive thermoelectric figure of merit (ZT) value. Specifically, we recorded a maximum ZT value of 1.09 at 363 K for the Fe-BTS sample containing 0.3 vol % of Fe nanometal decoration.

In essence, our study not only reveals the intricate dynamics of nanometal decoration and SPS processes in determining the thermoelectric behavior of Fe-BTS samples but also emphasizes the critical role of interface manipulation as a strategic avenue for enhancing thermoelectric properties. This nuanced understanding opens avenues for future advancements in the field of thermoelectric materials by providing valuable insights into the mechanisms controlling their performance.

■ ASSOCIATED CONTENT

Supporting Information

The Supporting Information is available free of charge at <https://pubs.acs.org/doi/10.1021/acsaem.4c01778>.

The SEM and EDS images of the fractured surfaces for the Fe-BTS samples (Fe 0, 0.1, 0.3, and 0.5 vol %), STEM-HAADF image and STEM-EDS image of the 0.1 vol % Fe-BTS sample, Magnetic hysteresis loops and saturation magnetization (M_s) at room temperature of Fe-BTS samples (Fe 0.1, 0.3, and 0.5 vol %) and The reproducibility of the 0.3 vol % Fe-BTS sample (PDF)

■ AUTHOR INFORMATION

Corresponding Authors

Jong Wook Roh – School of Nano & Materials Science and Engineering, Kyungpook National University, Gyeongsangbuk-do 37224, Republic of Korea; orcid.org/0000-0002-4730-2183; Email: jw.roh@knu.ac.kr

Wooyoung Lee – Department of Materials Science and Engineering, Yonsei University, Seoul 03722, Republic of Korea; orcid.org/0000-0001-8406-4324; Email: wooyoung@yonsei.ac.kr

Authors

Kyungmi Lee – Department of Materials Science and Engineering, Yonsei University, Seoul 03722, Republic of Korea

Gwansik Kim – E-drive Materials Research Team, Hyundai Motor Group, Uiwang-si, Gyeonggi-do 16082, Republic of Korea

Sung Wook Ye – School of Nano & Materials Science and Engineering, Kyungpook National University, Gyeongsangbuk-do 37224, Republic of Korea

Jeongmin Kim – DGIST, 333 Techno Jungang-daero, Hyeonpung-eup, Dalseong-gun, Daegu 42988, Republic of Korea

Complete contact information is available at:

<https://pubs.acs.org/10.1021/acsaem.4c01778>

Author Contributions

K.L. and G.K. contributed equally for this work. K.L. contributed to conceptualization, investigation, methodology and writing—original draft. G.K. contributed to conceptualization, investigation, methodology, writing—original draft and writing—review & editing. S.W.Y. contributed to formal analysis. J.K. contributed to formal analysis. J.W.R. contributed to supervision, conceptualization, methodology, writing—review & editing. W.L. contributed to supervision, project administration, writing—review & editing.

Notes

The authors declare no competing financial interest.

ACKNOWLEDGMENTS

This study was supported by the Technology Innovation Program [program no. 20013621, Center for Super Critical Material Industrial Technology] funded by the Ministry of Trade, Industry & Energy (MOTIE, Korea) and the Basic Science Research Program through the National Research Foundation of Korea (NRF) funded by the Ministry of Education [NRF2019R1A6A1A11055660]. J.W.R. gratefully acknowledges support from the National Research Foundation of Korea [grant numbers: NRF-2021R1A5A8033165 and NRF-2022R1A2C1007220].

REFERENCES

- (1) Kim, G.; Lee, K.; Shin, H.; Kim, J.; Chang, J.; Roh, J. W.; Lee, W. Strong enhancement of room-temperature thermoelectric properties of Cu-doped $\text{Bi}_2\text{Te}_{2.7}\text{Se}_{0.3}$. *Appl. Phys. Lett.* **2022**, *120*, 043903.
- (2) Kim, K.; Kim, G.; Lee, H.; Lee, K. H.; Lee, W. Band engineering and tuning thermoelectric transport properties of p-type $\text{Bi}_{0.52}\text{Sb}_{1.48}\text{Te}_3$ by Pb doping for low-temperature power generation. *Scr. Mater.* **2018**, *145*, 41–44.
- (3) Kim, G.; Lee, H.; Rim, H. J.; Kim, J.; Kim, K.; Roh, J. W.; Choi, S. M.; Kim, B. W.; Lee, K. H.; Lee, W. Dependence of mechanical and thermoelectric properties of $\text{Mg}_2\text{Si-Sn}$ nanocomposites on interface density. *J. Alloys Compd.* **2018**, *769*, 53–58.
- (4) Kim, G.; Kim, H. S.; Lee, H. S.; Kim, J.; Lee, K. H.; Roh, J. W.; Lee, W. Synchronized enhancement of thermoelectric properties of higher manganese silicide by introducing Fe and Co nanoparticles. *Nano Energy* **2020**, *72*, 104698.
- (5) Kim, S. I.; Lee, K. H.; Mun, H. A.; Kim, H. S.; Hwang, S. W.; Roh, J. W.; Yang, D. J.; Shin, W. H.; Li, X. S.; Lee, Y. H.; Snyder, G. J.; Kim, S. W. Dense dislocation arrays embedded in grain boundaries for high-performance bulk thermoelectrics. *Science* **2015**, *348* (6230), 109–114.
- (6) Jiang, J.; Chen, L. D.; Bai, S. Q.; Yao, Q.; Wang, Q. Fabrication and thermoelectric performance of textured n-type $\text{Bi}_2(\text{Te,Se})_3$ by spark plasma sintering. *Mater. Sci. Eng., B* **2005**, *117* (3), 334–338.
- (7) Meröz, O.; Gelbstein, Y. Thermoelectric $\text{Bi}_2\text{Te}_{3-x}\text{Se}_x$ alloys for efficient thermal to electrical energy conversion. *Phys. Chem. Chem. Phys.* **2018**, *20* (6), 4092–4099.
- (8) Pan, Y.; Aydemir, U.; Sun, F. H.; Wu, C. F.; Chasapis, T. C.; Snyder, G. J.; Li, J. F. Self-Tuning n-Type $\text{Bi}_2(\text{Te,Se})_3/\text{SiC}$ Thermoelectric Nanocomposites to Realize High Performances up to 300 °C. *Adv. Sci.* **2017**, *4* (11), 1700259.
- (9) Yan, X. A.; Poudel, B.; Ma, Y.; Liu, W. S.; Joshi, G.; Wang, H.; Lan, Y. C.; Wang, D. Z.; Chen, G.; Ren, Z. F. Experimental Studies on Anisotropic Thermoelectric Properties and Structures of n-Type $\text{Bi}_2\text{Te}_{2.7}\text{Se}_{0.3}$. *Nano Lett.* **2010**, *10* (9), 3373–3378.
- (10) El-Makaty, F.; Hamouda, A. M.; Abutaha, A.; Youssef, K. Optimization of the Consolidation Parameters for Enhanced Thermoelectric Properties of Gr- $\text{Bi}_2\text{Te}_{2.55}\text{Se}_{0.45}$ Nanocomposites. *Nanomaterials* **2024**, *14* (3), 260.
- (11) Kang, S. M.; Lee, K. H.; Roh, J. W.; Cho, H.; Park, S.; Park, J.; Kim, S. I. Enhanced Thermoelectric Properties in Highly Co-Doped Bi_2Se_3 by Density-of-State Effective Mass Increase. *Int. J. Energy Res.* **2024**, *2024*, 1–8.
- (12) Yang, G.; Sang, L.; Mitchell, D. R. G.; Fei Yun, F.; Wai See, K.; Jumlat Ahmed, A.; Sayyar, S.; Bake, A.; Liu, P.; Chen, L.; Yue, Z.; Cortie, D.; Wang, X. Enhanced thermoelectric performance and mechanical strength of n-type BiTeSe materials produced via a composite strategy. *Chem. Eng. J.* **2022**, *428*, 131205.
- (13) Li, L.; Wei, P.; Yang, M. J.; Zhu, W. T.; Nie, X. L.; Zhao, W. Y.; Zhang, Q. J. Strengthened interlayer interaction and improved room-temperature thermoelectric performance of Ag-doped n-type $\text{Bi}_2\text{Te}_{2.7}\text{Se}_{0.3}$. *Sci. China Mater.* **2023**, *66* (9), 3651–3658.
- (14) Li, Y. Z.; Zhang, Q.; Liu, K.; Lin, Y. J.; Lin, N.; Yu, Y.; Liu, F.; Zhao, X. B.; Ge, B. H.; Cojocar-Mirédin, O.; Fu, C. G.; Zhu, T. J. Multi-scale hierarchical microstructure modulation towards high room temperature thermoelectric performance in n-type Bi_2Te_3 -based alloys. *Mater. Today Nano* **2023**, *22*, 100340.
- (15) Zheng, J. Q.; Wang, D. Y.; Zhao, L. D. Enhancing thermoelectric performance of n-type $\text{Bi}_6\text{Cu}_2\text{Se}_4\text{O}_6$ through introducing transition metal elements. *Scr. Mater.* **2021**, *202*, 114010.
- (16) Zhu, B.; Huang, Z. Y.; Wang, X. Y.; Yu, Y.; Gao, N.; Zu, F. Q. Enhanced thermoelectric properties of n-type direction solidified $\text{Bi}_2\text{Te}_{2.7}\text{Se}_{0.3}$ alloys by manipulating its liquid state. *Scr. Mater.* **2018**, *146*, 192–195.
- (17) Wang, S. Y.; Tan, G. J.; Xie, W. J.; Zheng, G.; Li, H.; Yang, J. H.; Tang, X. F. Enhanced thermoelectric properties of $\text{Bi}_2(\text{Te}_{1-x}\text{Se}_x)_3$ -based compounds as n-type legs for low-temperature power generation. *J. Mater. Chem.* **2012**, *22* (39), 20943–20951.
- (18) Wu, X. K.; Wang, Z. Y.; Liu, Y.; Sun, X. L.; Xu, Y. F.; Tian, Y.; Wang, B.; Sang, X. H.; Shi, J.; Xiong, R. Enhanced performance of Bi_2Te_3 -based thermoelectric materials by incorporating $\text{Bi}_2\text{Fe}_4\text{O}_9$ magnetic nanoparticles. *J. Alloys Compd.* **2022**, *904*, 163933.
- (19) Zhao, W.; Liu, Z.; Wei, P.; Zhang, Q.; Zhu, W.; Su, X.; Tang, X.; Yang, J.; Liu, Y.; Shi, J.; Chao, Y.; Lin, S.; Pei, Y. Magnetoelectric interaction and transport behaviours in magnetic nanocomposite thermoelectric materials. *Nat. Nanotechnol.* **2017**, *12* (1), 55–60.
- (20) Wei, Z. C.; Wang, C. Y.; Zhang, J. Y.; Yang, J.; Li, Z. L.; Zhang, Q. D.; Luo, P. F.; Zhang, W. Q.; Liu, E. K.; Luo, J. Precise Regulation of Carrier Concentration in Thermoelectric BiSbTe Alloys via Magnetic Doping. *ACS Appl. Mater. Interfaces* **2020**, *12* (18), 20653–20663.
- (21) Wu, X. K.; Wang, Z. Y.; Zhang, Z. H.; Liu, Y.; Shi, J.; Xiong, R. Enhanced thermoelectric performance of N-type $\text{Bi}_2\text{Te}_{2.7}\text{Se}_{0.3}$ -based materials by superparamagnetic Fe_3O_4 nanoparticles. *Ceram. Int.* **2023**, *49* (5), 8271–8280.
- (22) Du, B. S.; Lai, X. F.; Liu, Q. L.; Liu, H. T.; Wu, J.; Liu, J.; Zhang, Z. H.; Pei, Y.; Zhao, H. Z.; Jian, J. K. Spark Plasma Sintered Bulk Nanocomposites of $\text{Bi}_2\text{Te}_{2.7}\text{Se}_{0.3}$ Nanoplates Incorporated Ni Nanoparticles with Enhanced Thermoelectric Performance. *ACS Appl. Mater. Interfaces* **2019**, *11* (35), 31816–31823.
- (23) Xie, W. H.; Wu, X. K.; Chen, Z.; Li, C.; Cao, W.; Wang, Z. Y. Enhancement of Thermoelectric Properties of p-Type $\text{Bi}_{0.4}\text{Sb}_{1.6}\text{Te}_3$ Incorporated by $\text{BaFe}_{12}\text{O}_{19}$ Magnetic Nanoparticles. *ACS Appl. Energy Mater.* **2023**, *6* (23), 12013–12021.
- (24) Zhu, C.; Wang, J.; Luo, F.; Zhang, S.; Wang, J. F.; Zhang, Y.; Liu, H. X.; Sun, Z. G. Enhanced Thermoelectric Performance of GeTe-Based Composites Incorporated with Fe Nanoparticles. *ACS Appl. Mater. Interfaces* **2022**, *14* (34), 38854–38864.
- (25) Hu, Q. J.; Guo, J. B.; Zuo, H. Y. Realize high thermoelectric properties in n-type $\text{Bi}_2\text{Te}_{2.7}\text{Se}_{0.3}$ materials via ZrO_2 ceramic

nanoparticles mediated heterogeneous interface. *Ceram. Int.* **2023**, *49* (11), 18371–18378.

(26) Xu, P. F.; Jin, K. P.; Yu, Y.; Huang, M.; Yan, Z. H.; Li, X.; Gao, X.; Fu, L. W.; Xu, B. High-Performance Bi₂Te₃-Based Thermoelectrics Enabled by ≈1 nm Metal Chalcogenide Clusters with Size-Dependent Electron and Phonon Structures. *Adv. Funct. Mater.* **2024**, *34*, 2401240.

(27) Zhao, Y. W.; Liu, Y.; Ma, H. Y.; Deng, S. P.; Wang, H. Y.; Xiong, R.; Huang, S. Enhancing the thermoelectric performance of CoSb₃-based skutterudite by decoupling the electrical and thermal properties by embedding Cu nanoparticles. *Ceram. Int.* **2021**, *47* (20), 28268–28273.

(28) Li, C. C.; Ma, S. F.; Wei, P.; Zhu, W. T.; Nie, X. L.; Sang, X. H.; Sun, Z. G.; Zhang, Q. J.; Zhao, W. Y. Magnetism-induced huge enhancement of the room-temperature thermoelectric and cooling performance of p-type BiSbTe alloys. *Energy Environ. Sci.* **2020**, *13* (2), 535–544.

(29) Zhao, Y.; Nie, X. L.; Sun, C. L.; Chen, Y. F.; Ke, S. Q.; Li, C. C.; Zhu, W. T.; Sang, X. H.; Zhao, W. Y.; Zhang, Q. J. Excellent Thermoelectric Performance from In Situ Reaction between Co Nanoparticles and BiSbTe Flexible Films. *ACS Appl. Mater. Interfaces* **2021**, *13* (49), 58746–58753.

(30) Faleev, S. V.; Leonard, F. Theory of enhancement of thermoelectric properties of materials with nano-inclusions. *Phys. Rev. B* **2008**, *77* (21), 214304.

(31) Joshi, G.; Lee, H.; Lan, Y.; Wang, X.; Zhu, G.; Wang, D.; Gould, R. W.; Cuff, D. C.; Tang, M. Y.; Dresselhaus, M. S.; Chen, G.; Ren, Z. Enhanced Thermoelectric Figure-of-Merit in Nanostructured p-type Silicon Germanium Bulk Alloys. *Nano Lett.* **2008**, *8* (12), 4670–4674.

(32) Lee, K. H.; Kim, H. S.; Kim, S. I.; Lee, E. S.; Lee, S. M.; Rhyee, J. S.; Jung, J. Y.; Kim, I. H.; Wang, Y. F.; Koumoto, K. Enhancement of Thermoelectric Figure of Merit for Bi_{0.5}Sb_{1.5}Te₃ by Metal Nanoparticle Decoration. *J. Electron. Mater.* **2012**, *41* (6), 1165–1169.

(33) Lin, Y.; Watson, K. A.; Fallbach, M. J.; Ghose, S.; Smith, J. G.; Delozier, D. M.; Cao, W.; Crooks, R. E.; Connell, J. W. Rapid, Solventless, Bulk Preparation of Metal Nanoparticle-Decorated Carbon Nanotubes. *ACS Nano* **2009**, *3* (4), 871–884.

(34) Jung, S. J.; Park, S. Y.; Kim, B. K.; Kwon, B.; Kim, S. K.; Park, H. H.; Kim, D. I.; Kim, J. Y.; Hyun, D. B.; Kim, J. S.; Baek, S. H. Hardening of Bi-Te based alloys by dispersing B₄C nanoparticles. *Acta Mater.* **2015**, *97*, 68–74.

(35) Pakdel, A.; Guo, Q. S.; Nicolosi, V.; Mori, T. Enhanced thermoelectric performance of Bi-Sb-Te/Sb₂O₃ nanocomposites by energy filtering effect. *J. Mater. Chem. A* **2018**, *6* (43), 21341–21349.

(36) Kim, M. Y.; Kim, D.; Kim, G.; Lee, W.; Perez, N.; Nielsch, K.; Shim, J. H.; Jin, H. Enhancing thermoelectric performance via relaxed spin polarization upon magnetic impurity doping. *J. Mater. Chem. A* **2023**, *11* (23), 12013–12024.

(37) Cho, H.; Back, S. Y.; Yun, J. H.; Byeon, S.; Jin, H.; Rhyee, J. S. Thermoelectric Properties and Low-Energy Carrier Filtering by Mo Microparticle Dispersion in an n-Type (CuI)_{0.003}Bi₂(Te,Se)₃ Bulk Matrix. *ACS Appl. Mater. Interfaces* **2020**, *12* (34), 38076–38084.

(38) Lee, K. H.; Kim, S. I.; Lim, J. C.; Cho, J. Y.; Yang, H.; Kim, H. S. Approach to Determine the Density-of-States Effective Mass with Carrier Concentration-Dependent Seebeck Coefficient. *Adv. Funct. Mater.* **2022**, *32* (33), 2203852.

(39) Cutler, M.; Leavy, J. F.; Fitzpatrick, R. L. Electronic transport in semimetallic cerium sulfide. *Phys. Rev.* **1964**, *133* (4A), A1143–A1152.

(40) Toberer, E. S.; Zevkink, A.; Snyder, G. J. Phonon engineering through crystal chemistry. *J. Mater. Chem.* **2011**, *21* (40), 15843–15852.

(41) Wilson, R. G. Vacuum thermionic work functions of polycrystalline Be, Ti, Cr, Fe, Ni, Cu, Pt, and type 304 stainless steel. *J. Appl. Phys.* **1966**, *37* (6), 2261–2267.

(42) Gayner, C.; Amouyal, Y. Energy Filtering of Charge Carriers: Current Trends, Challenges, and Prospects for Thermoelectric Materials. *Adv. Funct. Mater.* **2020**, *30* (18), 1901789.

(43) Cho, H.; Yun, J. H.; Kim, J. H.; Back, S. Y.; Lee, H. S.; Kim, S. J.; Byeon, S.; Jin, H.; Rhyee, J. S. Possible Charge Density Wave and Enhancement of Thermoelectric Properties at Mild-Temperature Range in n-Type CuI-Doped Bi₂Te_{2.1}Se_{0.9} Compounds. *ACS Appl. Mater. Interfaces* **2020**, *12* (1), 925–933.

(44) Narducci, D.; Selezneva, E.; Cerofolini, G.; Frabboni, S.; Ottaviani, G. Impact of energy filtering and carrier localization on the thermoelectric properties of granular semiconductors. *J. Solid State Chem.* **2012**, *193*, 19–25.

(45) Kim, H. S.; Kim, T.; An, J.; Kim, D.; Jeon, J. H.; Kim, S. I. Segregation of NiTe₂ and NbTe₂ in p-Type Thermoelectric Bi_{0.5}Sb_{1.5}Te₃ Alloys for Carrier Energy Filtering Effect by Melt Spinning. *Appl. Sci.* **2021**, *11* (3), 910.

(46) Kawajiri, Y.; Tanusilp, S. A.; Kumagai, M.; Ishimaru, M.; Ohishi, Y.; Tanaka, J.; Kurosaki, K. Enhancement of Thermoelectric Properties of n-Type Bi₂Te_{3-x}Se_x by Energy Filtering Effect. *ACS Appl. Energy Mater.* **2021**, *4* (10), 11819–11826.

(47) Kim, H. S.; Gibbs, Z. M.; Tang, Y. L.; Wang, H.; Snyder, G. J. Characterization of Lorenz number with Seebeck coefficient measurement. *APL Mater.* **2015**, *3* (4), 041506.

(48) Mun, H.; Choi, S. M.; Lee, K. H.; Kim, S. W. Boundary Engineering for the Thermoelectric Performance of Bulk Alloys Based on Bismuth Telluride. *ChemSusChem* **2015**, *8* (14), 2312–2326.